Molecular Cell
Article

Dynamic Protein-Protein Interaction Wiring of the Human Spliceosome

Anna Hegele,[1,3] Atanas Kamburov,[1,3] Arndt Grossmann,[1] Chrysovalantis Sourlis,[1] Sylvia Wowro,[1] Mareike Weimann,[1] Cindy L. Will,[2] Vlad Pena,[2] Reinhard Lührmann,[2] and Ulrich Stelzl[1,*]
[1]Otto-Warburg Laboratory, Max-Planck Institute for Molecular Genetics (MPI-MG), 14195 Berlin, Germany
[2]Department of Cellular Biochemistry, Max-Planck Institute of Biophysical Chemistry (MPI-BPC), 37077 Göttingen, Germany
[3]These authors contributed equally to this work
*Correspondence: stelzl@molgen.mpg.de
DOI 10.1016/j.molcel.2011.12.034

SUMMARY

More than 200 proteins copurify with spliceosomes, the compositionally dynamic RNPs catalyzing pre-mRNA splicing. To better understand protein - protein interactions governing splicing, we systematically investigated interactions between human spliceosomal proteins. A comprehensive Y2H interaction matrix screen generated a protein interaction map comprising 632 interactions between 196 proteins. Among these, 242 interactions were found between spliceosomal core proteins and largely validated by coimmunoprecipitation. To reveal dynamic changes in protein interactions, we integrated spliceosomal complex purification information with our interaction data and performed link clustering. These data, together with interaction competition experiments, suggest that during step 1 of splicing, hPRP8 interactions with SF3b proteins are replaced by hSLU7, positioning this second step factor close to the active site, and that the DEAH-box helicases hPRP2 and hPRP16 cooperate through ordered interactions with GPKOW. Our data provide extensive information about the spliceosomal protein interaction network and its dynamics.

INTRODUCTION

Pre-mRNA splicing is catalyzed by the spliceosome, a highly complex, dynamic, and protein-rich ribonucleoprotein complex (RNP) that assembles de novo on each intron to be spliced. During spliceosome assembly, activation, catalysis, and disassembly defined large RNP complexes are formed in an ordered, stepwise manner (for reviews see [Smith et al., 2008; Wahl et al., 2009]). The U1 snRNP binds the 5′ splice site (ss) of the pre-mRNA, and after branchpoint recognition by the U2 snRNP, the A complex is formed. Then, the U5°U4/U6 tri-snRNP joins, generating the B complex. The B complex is activated in a subsequent step involving large rearrangements in which the U1 and U4 snRNPs are destabilized or released, yielding the Bact complex. Subsequently, after a structural rearrangement is triggered by the ATP-dependent DEAH-box protein PRP2 (Gencheva et al., 2010; Warkocki et al., 2009), the catalytically activated spliceosome (i.e., the B* complex) is formed. The B* complex is then converted into the C complex, in which the first of the two catalytic steps of splicing has occurred. During this step, the pre-mRNA is cleaved at the 5′ss and a lariat-like structure is formed by the intron and the 3′ exon. The action of a second ATP-dependent DEAH-box protein, PRP16, promotes the second catalytic step (Schwer and Guthrie, 1991; Zhou and Reed, 1998), in which the two exons are ligated. The spliced intron is then released, the spliceosome dissociates, and the snRNPs are recycled for additional rounds of splicing.

A dynamic network of RNA-RNA interactions plays an import role in splicing (Staley and Guthrie, 1998). However, during the course of the splicing cycle the protein composition of the spliceosome is also highly dynamic (Jurica and Moore, 2003; Wahl et al., 2009), with dynamic RNA-protein and protein-protein interactions crucial for the formation, rearrangement, and dissociation of the spliceosomal complexes (Smith et al., 2008; Staley and Guthrie, 1998). Analysis of the protein composition of individual human spliceosomal complexes (i.e., A, B, Bact, and C) by mass spectrometry (MS) has shown a large exchange of proteins at most stages of splicing. For example, during the transition from B to Bact, at least 30 proteins present in B complexes are destabilized or released and approx. 35 proteins are recruited or are more stably associated with the spliceosome, including the Prp19 complex and the group of Prp19-related proteins (Bessonov et al., 2008). Another set of more than 40 proteins exchanges during the conversion of the human Bact to C complex (Bessonov et al., 2010).

More than 200 proteins are associated at one or more stages with human spliceosomes assembled on prototype pre-mRNAs in cellular extracts (reviewed by [Jurica and Moore, 2003; Wahl et al., 2009]). This number includes 141 proteins designated as core components of the human spliceosome, based on their high abundance (Agafonov et al., 2011) or known function in splicing, as well as proteins specifically associated with the U1, U2, U5, U4/U6 snRNPs, or the U5°U4/U6 tri-snRNP (Figure 1). There is also a set of more than 100 noncore proteins, including mRNA binding and regulatory proteins, such as hnRNPs and SR-rich splicing factors, that presumably link the spliceosome to other cellular machineries such as transcription factors, as well as proteins that copurify reproducibly but are present in very low amounts (Agafonov et al., 2011).

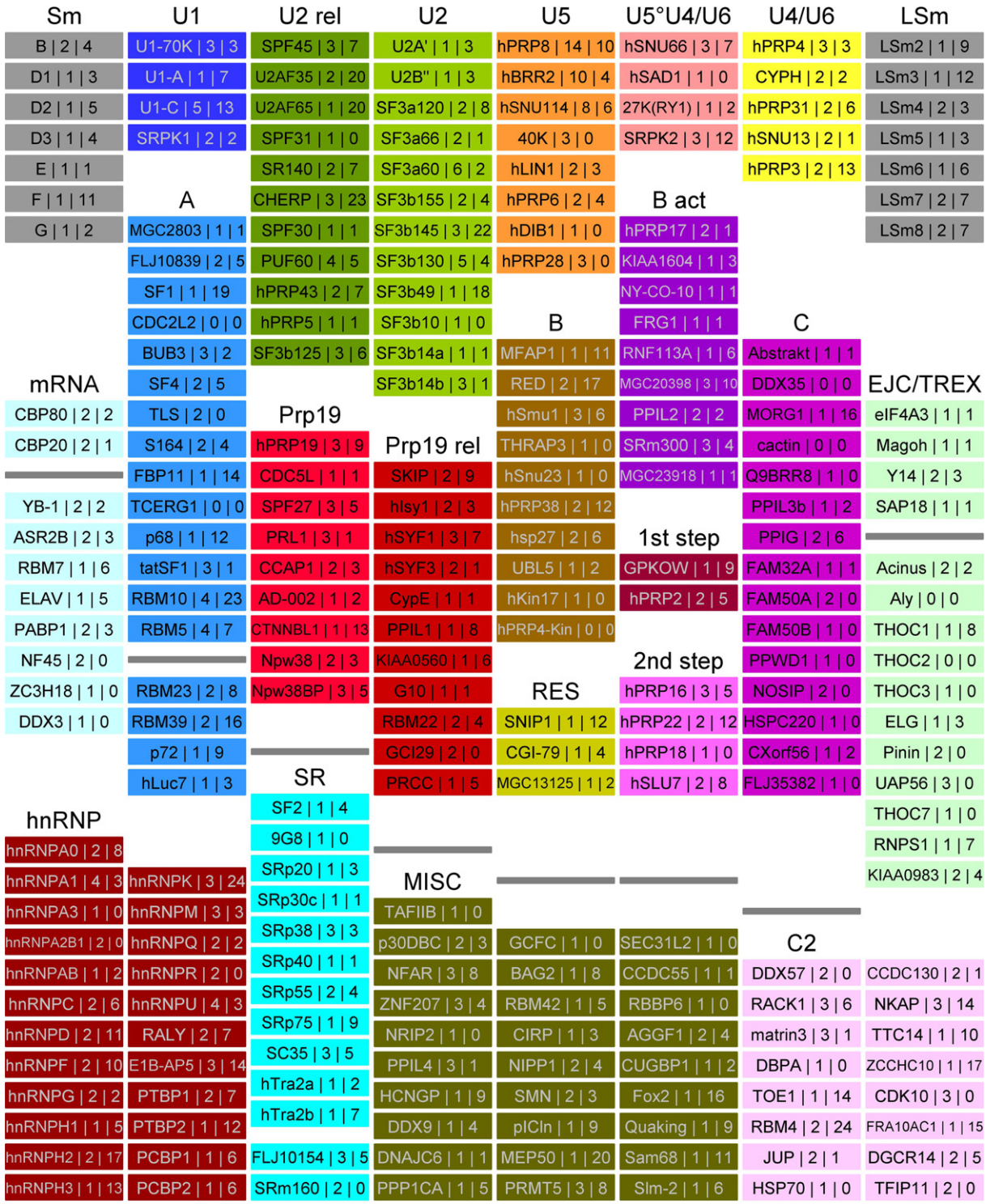

Figure 1. Overview of the Spliceosomal Proteome

Human proteins (244) that copurify with defined spliceosomal complexes are named according to the commonly used nomenclature (Wahl et al., 2009) and grouped (each group color-coded) according to their presence in a given complex or their function. They are also classified into core and noncore proteins (above and below the gray bar, respectively) primarily based on their abundance in spliceosomal complexes (Agafonov et al., 2011). The pipes (|) separate the number of clones used and the number of PPIs found with the protein in the Y2H matrix screen. For 237 proteins, at least 1 clone was tested in the Y2H matrix screen, and for 196 proteins, at least 1 PPI was detected. A comprehensive overview of the proteins and clones, including, e.g., standard identifiers such as NCBI gene names, can be found in Tables S1 and S2.

The complexity of the splicing process, its structural and compositional dynamics, and the large number of protein components involved dictates that protein-protein interactions (PPIs) be investigated systematically at a scale that involves all spliceosomal proteins. High-throughput approaches have been implemented to reliably determine PPIs at a genomic scale (reviewed in [Sanderson, 2009; Stelzl and Wanker, 2006]), as well as in more focused approaches analyzing, for example, aspects of RNA processing in yeast (Fromont-Racine et al., 1997) and humans (Lehner and Sanderson, 2004). Here we systematically investigated PPIs among 244 human spliceosomal core and noncore proteins using a Y2H interaction matrix screening approach. We obtained a high-quality PPI map that recapitulates very well-known protein associations. In total, 632 interactions were detected, with 242 found between human spliceosomal core proteins. A large fraction of the latter interactions could be validated by coimmunoprecipitation (co-IP) experiments. We also investigated dynamic changes in PPIs during splicing using an integrative clustering approach and co-IP competition assays. The dynamic interaction patterns identified provide the basis for mechanistic hypotheses addressing rearrangements during the transition from the B to C complex and the action of DEAH-box helicases during the catalytic steps of splicing.

RESULTS

Pairwise PPI Screening of Human Spliceosomal Proteins

To systematically analyze human spliceosomal PPIs, we set out to clone all 244 proteins reported to associate with the human spliceosome in studies that characterized the protein repertoire of functional A, B, Bact, and C spliceosomal complexes for yeast two-hybrid (Y2H) protein interaction analyses (Figure 1 and Table S1 available online). In total, 237 proteins were represented by 442 clones in our study (Table S2). Typically, we obtained one or two full-length clones for each protein (Figures 1 and 2A); additionally, larger proteins, such as the U5 proteins hPRP8 (220 kDa) or hBRR2 (200 kDa), were divided up into multiple fragments based on size or domain annotation (Figure 2B). All cDNAs were cloned into Gateway Entry vectors and transferred to Y2H-bait and prey vectors for pairwise protein interaction testing.

We used a well-controlled, stringent, automated, yeast two-hybrid setup that allowed the generation of systematic PPI data with high precision (Stelzl et al., 2005; Venkatesan et al., 2009; Vinayagam et al., 2011). Because all proteins used in the screen were purified with bona fide spliceosomal complexes, the fraction of false positive interactions was expected to be very low (Schwartz et al., 2009). Furthermore, the use of several different clones per protein should reduce the false-negative rate (Venkatesan et al., 2009). Initially, several baits representing the same proteins were pooled and screened three times against the matrix of all preys (Figure 2C and Table S2). Baits that did not show any interactions or, conversely, resulted in a set of well-sampled PPIs in the first three screens were not tested further. The others were screened additionally, up to six times, using individual bait clones to obtain a high coverage of interacting bait- and prey pairs. Altogether 400,000 pairwise interaction tests were carried out. A total of 3,003 positive colonies from 1,224 bait-prey pairs were found to interact in at least two experiments. PPIs detected with multiple combinations of clones and bait-prey orientations were combined using a probabilistic Y2H score reflecting the success rate of how often a protein pair was found to interact in the screen (Figure 2D). Our screen revealed 632 unique PPIs between 196 proteins with a Y2H score between 0.33 and 1 (Table S3). Among these, 390 PPIs involved noncore proteins, whereas 242 PPIs were found between spliceosomal core proteins.

Comparison to PPIs in the Literature

Many well-studied binary interactions with known roles in splicing were recapitulated in our screen. Examples include interactions between the U2 snRNP proteins SF3a120–SF3a60 (Nesic and Krämer, 2001), as well as the tri-snRNP proteins hPRP6–hPRP31 (Liu et al., 2006) or the EJC complex proteins Y14–Magoh (Gehring et al., 2009). However, closer inspection of the literature revealed that a high fraction of database-annotated spliceosomal PPIs were not assessed in binary interaction assays, such as Y2H, GST-pulldown, pairwise co-IP, and far western, or observed in 3D structure-determination experiments. Rather, many PPIs were inferred from copurification experiments of larger complexes. To address this problem, we used the ConsensusPathDB meta-database, which comprehensively collects human PPIs from heterogeneous interaction data resources (Kamburov et al., 2011), to search for reported interactions among spliceosomal proteins. We manually re-evaluated 898 PPI entries reported in 245 publications to distinguish binary interactions from copurification evidence. A collection of 311 binary reference PPIs (including 38 homodimers) reported in 201 papers was retrieved (Table S4). Direct comparison of our data set with the reference interactions shows an overlap of 72 PPIs for the entire PPI data set and 43 for PPIs involving solely core proteins (Figure 3A). The coverage, (i.e., the fraction of known PPIs retrieved in the Y2H screen) is 26% and 41% for the entire PPI data and for core-protein interactions, respectively. This is one of the lowest false-negative rates reported for a systematic PPI screen (Venkatesan et al., 2009). The higher coverage for the 141 core proteins may be explained by the relatively fewer direct PPIs known and the fact that more clones were used in our Y2H assays for core versus noncore proteins (on average, 2 and 1.7 clones per protein, respectively). Importantly, for 89 proteins analyzed in our screen, we recapitulated PPIs found in the binary reference set. On average, 12% (all spliceosomal proteins) and 19% (core proteins) of our interactions were reported previously. As shown in Figure 3A, our data set expands the number of spliceosomal PPIs by 200%.

We next tested whether proteins belonging to the same operationally defined group (Figure 1) interact preferentially with each other. We generated 1,000 randomly rewired networks by shuffling the interactions but keeping the number of interactions for each protein as in the experimental network. Preferentially interacting groups of proteins were determined based on their z-score (Figure 3B). Indeed, we observed a strong enrichment for interactions between proteins belonging to the same operationally defined group of spliceosomal proteins (Figure 3B, green bars). Other preferentially interacting groups of proteins, such as A complex proteins with U2-related proteins, B and Bact

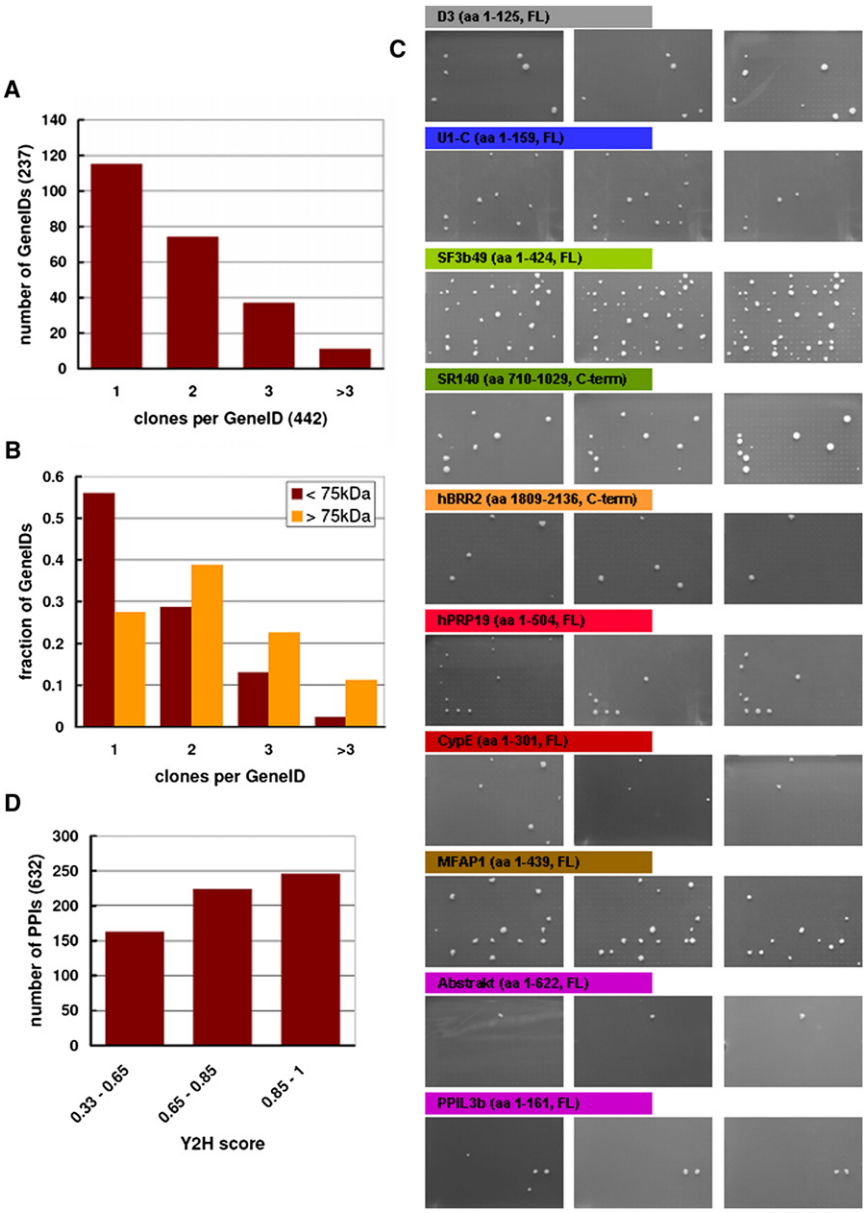

Figure 2. Systematic Y2H Interaction Matrix Screening

(A) The number of clones per GeneID: 442 clones representing 237 proteins were used for PPI analysis. The majority of proteins were covered with one or two full-length cDNAs.

(B) Distribution of the number of clones per GeneID. Proteins larger than 75kDa were typically covered by more clones, including cDNA fragments and domain-based constructs, than smaller proteins (<75kDa).

(C) Representative sections of selective Y2H plates from three independent screens for the indicated bait proteins (one plate with 384 tested pairs each). Colonies indicate an interacting bait-prey pair. Pairs that grew in at least two independent screens were considered for statistical data evaluation.

(D) Y2H score distribution for 632 unique PPIs reported in this study. A Y2H score was calculated which reflected the success rate of how often an unique protein pair was found to interact in different replicas using different clones and different Y2H configurations (see Table S3).

complex proteins with U5 proteins, or Bact proteins with Prp19-related proteins, also agree with the current structural and functional view of the human spliceosome (Figure 3B, orange bars). Furthermore, core and noncore spliceosomal proteins are significantly less connected between each other than within each group (Table S5), concurring with our initial knowledge-based classification of core and noncore proteins.

Validation of Y2H Interactions via Coimmunoprecipitation Assays

To validate our Y2H PPIs, we focused on spliceosomal core proteins and systematically tested their interactions in luciferase based co-IP experiments with transiently expressed proteins. Because different interaction assays are, by nature, complementary, we do not expect that only those interactions found in both the Y2H and the co-IP approach will prove meaningful (Sanderson, 2009; Stelzl and Wanker, 2006). However, considering that each assay has its false-positive and false-negative rates, we can use the co-IP assay to benchmark the Y2H data set (Venkatesan et al., 2009). Moreover, an interaction that is observed with both assays—although not more relevant per se—is less likely to be false positive.

We tested a total of 171 core PPIs in co-IP experiments (Figure 3C and Table S3). Among these,16 protein pairs did not give useful results because proteins either were not expressed to detectable levels, or background binding to the IgG-coated plates was prohibitively high. We confirmed 109 interactions in at least one orientation in the co-IP assay, whereas 46 interacting pairs did not bind reproducibly under the conditions used. Importantly, PPIs reported previously were coprecipitated with a very similar success rate (12/17 were positive, Figure 3C). We also tested a set of 96 spliceosomal protein pairs that did not interact in the Y2H screen for interaction in the co-IP assay. The success rate for Y2H noninteracting pairs was much lower than for Y2H PPIs (19/96 were positive, Figure 3C). The results underscore the high quality of our PPI dataset and are presented in full in Table S6.

PPIs between Spliceosomal Core Proteins

We have identified more than 500 previously unknown interactions between spliceosomal proteins (Figure 3A and Table S3), 188 of which are between core proteins and, thus, likely to play

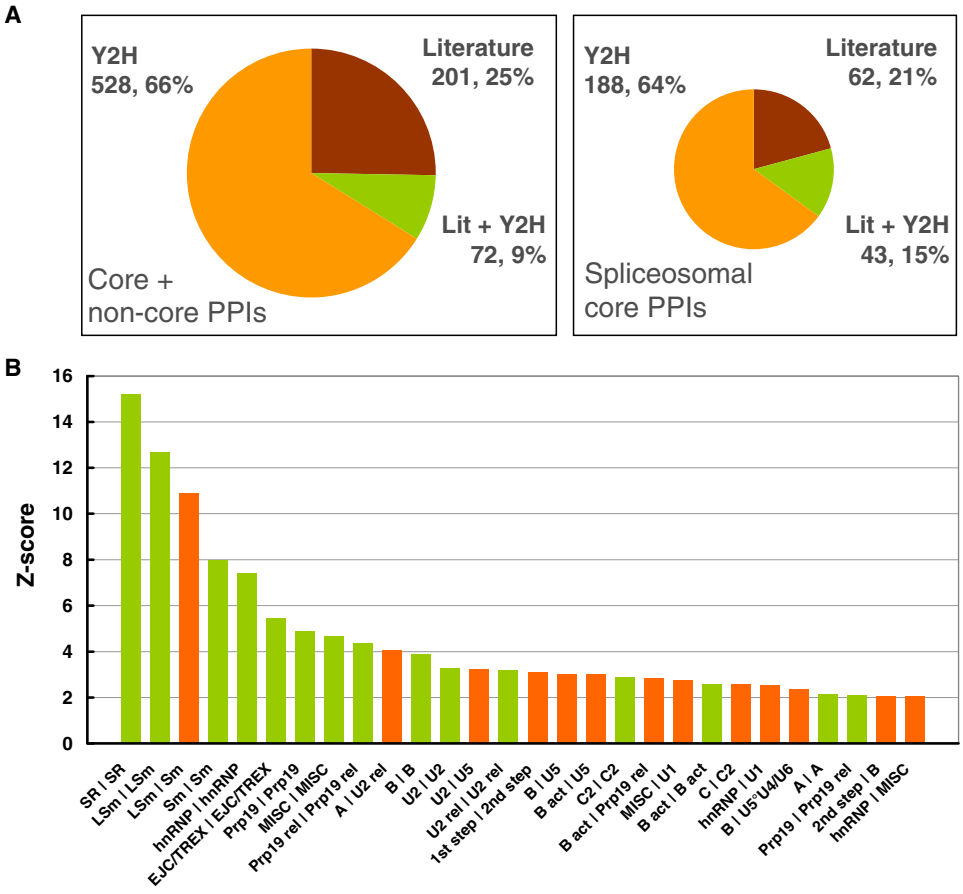

C

Data set	# PPIs tested	# PPIs positive	# PPIs negative	# PPIs not determined	Success rate [%]
Y2H PPIs	171	109	46	16	70
Y2H PPIs known from Literature	17	12	5	0	70
Y2H non-interacting pairs	96	19	77	0	20

Figure 3. Knowledge-Based Assessment of the Y2H PPI Data

(A) Comparison of the Y2H PPI data with reported binary PPIs: 201 publications that report 273 human PPIs with at least 1 assay indicative of a binary physical interaction were re-evaluated (excluding self-interactions); 72 and 43 PPIs have been recapitulated for the whole and the core-protein data set, corresponding to coverage values of 26% and 41%, respectively. The analysis did not account for PPIs that have been reported with conserved protein pairs in yeast or other model organisms.

(B) Enrichment analysis for interactions according to the functional annotation of the proteins. Proteins from the same functional group interacted preferentially (green bars). Some groups also showed specific PPI enrichment with other groups (orange bars). Enrichment was calculated by comparing with 1,000 randomly rewired networks, keeping the number of interactions for each protein constant. All enriched-group pairs with a z-score greater than 2 are shown.

(C) Co-IP results: 171 PPIs involving core spliceosomal proteins were tested in co-IP assays with a success rate of 70%. The subset of PPIs that were also reported in the literature shows a similar success rate in our assay. Randomly selected pairs of spliceosomal proteins that did not interact in the Y2H assay showed a success rate of 20%. However, this is not an estimate for the false-positive rate of the co-IP assay because these proteins are much more likely to interact than unbiased random control noninteracting pairs.

important roles in the assembly/stability of a given spliceosomal complex or in the recruitment of spliceosomal subcomplexes. The remaining interactions involve noncore proteins and are discussed elsewhere (see Figure S4 and Discussion).

Our network analysis indicated that A and U2-related proteins (also present in A complexes) preferentially interact (Figure 3B). For example, the U2-related protein SPF45 plays an important role in the regulation of alternative splicing via PPIs with SF3b155 and the branchpoint-binding protein SF1 (Corsini et al., 2007). We recapitulated these interactions and found that SPF45 additionally binds SF4, another A complex protein, and hPRP43, a DEAH helicase protein of the U2-related group.

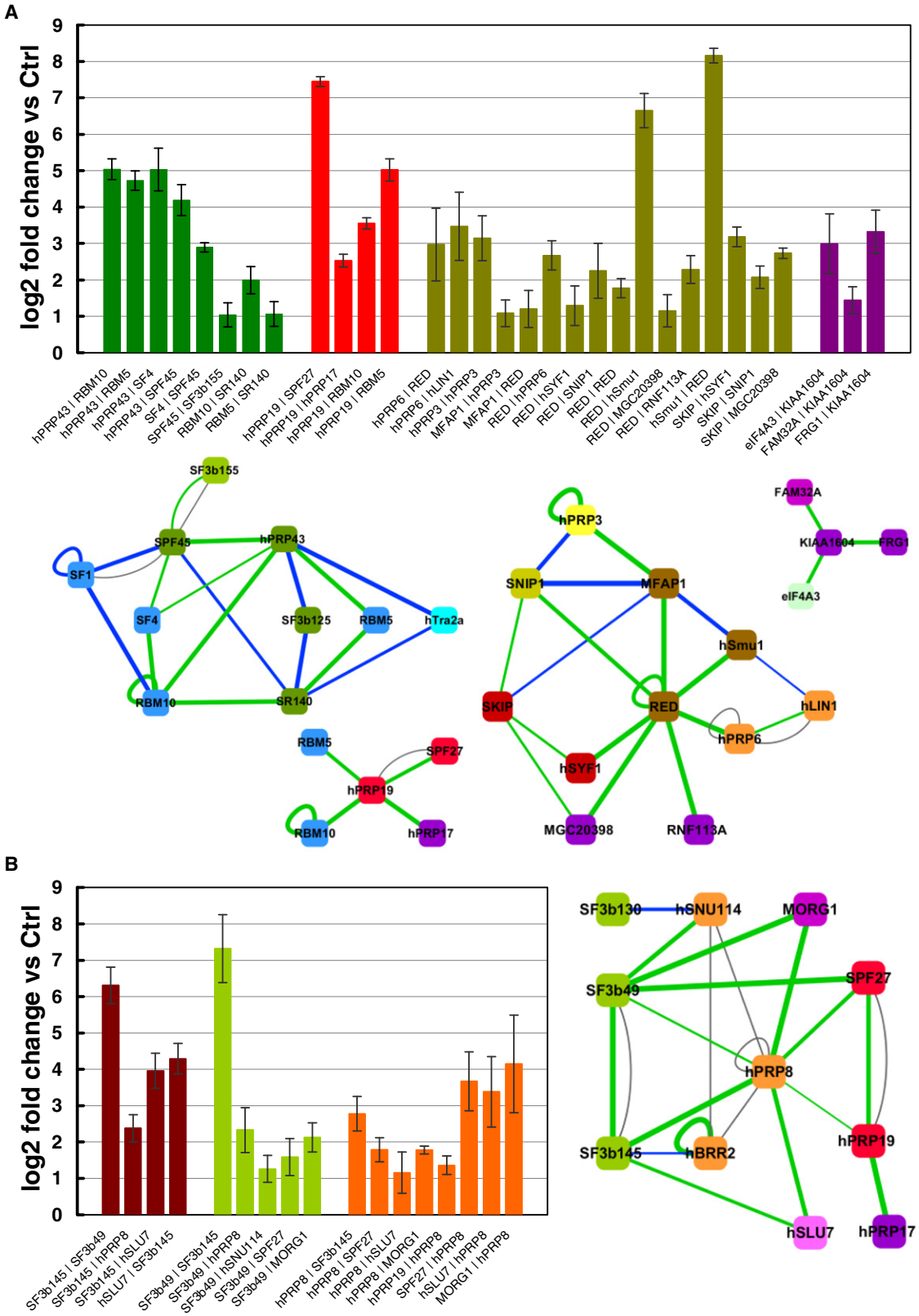

Figure 4. Validation of Y2H PPIs through co-IP Assays

(A and B) Co-IP results for groups of interacting proteins centered around 1) the SPF45–hPRP43 interacting pair, 2) hPRP19, 3) the interacting B proteins MFAP1–RED–hSmu1, 4) KIAA1604 (A) and the SF3b–U5 protein interactions (B). Log_2-fold binding compared to control in co-IP experiments for the indicated protein pairs

Together with SR140, a cluster of PPIs (Figure 4A) suggests that U2-related proteins such as SPF45 and hPRP43 play a prominent role in the A complex.

Little is known about PPIs important for tri-snRNP recruitment during B complex formation. We detect several PPIs that may play a key role in this process. The U5 proteins hPRP8, hBRR2, and hSNU114, which interact with each other (Liu et al., 2006; Pena et al., 2007), are major core components of the spliceosome that play essential roles at several steps of splicing (Abelson, 2008; Wahl et al., 2009). Because these proteins are exceptionally large, we screened 12 hPRP8, 8 hBRR2, and 7 hSNU114 fragments for PPIs. The majority of these did not show any interactions, most likely because they were not expressed or not folded properly (Figure S1). However, using hPRP8 constructs that resembled folded domains previously characterized in structural studies (e.g., comprising the RNase H-like domain [designated hPrp8 core] and/or the MPN domain) (Pena et al., 2007, 2008; Ritchie et al., 2008; Yang et al., 2008), we mapped contacts with several other spliceosomal core components (Figures 4B and S1). Significantly, we observed interactions between the three major U5 proteins and three components of the SF3b complex, namely hBRR2 - SF3b145, hPRP8–SF3b145, hPRP8–SF3b49, hSNU114–SF3b49, and hSNU114–SF3b130 (Figure 4B). Additionally, PPIs were observed between hSLU7, an important second step factor (Chua and Reed, 1999) and both SF3b145 and hPRP8, and also between MORG1, a protein first abundant in the C complex (Bessonov et al., 2010) and both SF3b49 and hPRP8. The identification of multiple PPIs involving hPRP8 is consistent with its large size (220KDa) and its central role as a scaffold protein within the spliceosome.

Little is known about which PPIs are important for the recruitment of the functionally important hPrp19 complex during B complex formation and its subsequent stabilization after activation. Our data confirm the previously reported interaction between hPRP19 and the Prp19 complex protein SPF27 (Grote et al., 2010) and also reveal that hPRP19 specifically binds RBM5 and RBM10, both present in A and B complexes (Agafonov et al., 2011) (Figure 4A). Likewise, SPF27 interacts with SF3b49, and both Prp19 and SPF27 interact with the U5 protein hPRP8 (Figure 4B). Thus, these PPIs may aid the initial recruitment of Prp19 and its associated proteins to the B complex. We also detect, via Y2H and co-IP, an interaction between hPRP19 and hPRP17 (Figure 4A), which concurs with data indicating that the yeast homologs of these proteins also interact (Ren et al., 2011). hPRP17, which is required for catalytic step 2 (Sapra et al., 2008; Zhou and Reed, 1998), is first abundant in the Bact complex (Bessonov et al., 2010) and could potentially contribute to the stable association of the Prp19 complex after spliceosome activation.

MFAP1, RED, and hSmu1 are abundant components of the human B complex but their role in splicing is not known. We demonstrate that these proteins interact directly not only with each other but also with U5 (hPRP6) and U4/U6 (hPRP3) proteins (Figure 4A), suggesting they may also play a role in tri-snRNP recruitment during B complex formation. We also detected PPIs between the RES complex protein SNIP1 and both RED and MFAP1, as well as between these proteins and the hPrp19-related proteins hSYF1 and SKIP (Figure 4A). Thus, MFAP, RED, and Smu-1 may aid in the recruitment of a variety of protein groups to the B complex, suggesting they play an important structural role at this stage of splicing.

Interactions were also found between KIAA1604, an abundant Bact and C complex protein of unknown function, and three proteins of the Bact and/or C complex, namely the EJC protein eIF4A3, FAM32A, and FRG1 (Figure 4A). While the role of FAM32A in the C complex is elusive, overexpression of FRG1 has been causally linked to facioscapulohumeral muscular dystrophy, an inherited putative splicing disorder (Gabellini et al., 2006). Thus, our PPI data provide a specific lead to investigate the function of this human disease protein.

Analysis of Dynamic PPI Patterns during Splicing

We collected protein composition data from 76 individual isolations of human spliceosomal complexes that were either published previously (mainly by the Lührmann laboratory) or are unpublished purifications of similar complexes from the Lührmann lab. Because most of these experiments do not provide quantitative information, we created a binary-complex purification table that indicates the presence or absence of a protein (rows) in a preparation (columns). Using this information, we calculated a copurification score for every possible pair of proteins tested in our Y2H screen (Figure S2), weighting the number of co-occurrences of two proteins. Higher copurification scores are given to proteins pairs involving proteins that are found rarely (i.e., in fewer complexes) and in more stringent preparations (i.e., in complexes with fewer proteins).

Next, we compared the copurification scores with our Y2H data. The average copurification score of interacting pairs is much higher than in randomized networks with the same size and degree distribution, keeping the number of interactions for each protein constant (z-score = 9.2, $p < 0.0001$; Figure 5A). This is an important result because it shows high agreement between our PPI screening data and the copurification data, which contains truly independent interaction information generated by an entirely different technique. Our Y2H data provide a wealth of binary information about physical contacts important for defining modules that build up these large multiprotein splicing complexes.

To identify PPI modules (i.e., groups of proteins that preferentially interact with each other), we applied an interaction clustering approach onto our network to reveal PPI modules (Pereira-Leal et al., 2004; Vlasblom and Wodak, 2009). Importantly, because interactions are clustered, a single protein can contribute interactions in several modules, revealing PPI

(the firefly-fusion protein is pipe-separated from the protein A-tagged protein) is shown. Error bars show the standard deviation from an experiment performed with triplicate transfections. Interacting pairs with at least 2-fold binding over background and z-scores of at least two were scored positive. Network illustrations of the results, with positive co-IP interactions highlighted in green, are shown below.Y2H interactions in blue, literature in gray (thickness of the line: Y2H score). For the full data set, see Table S6.

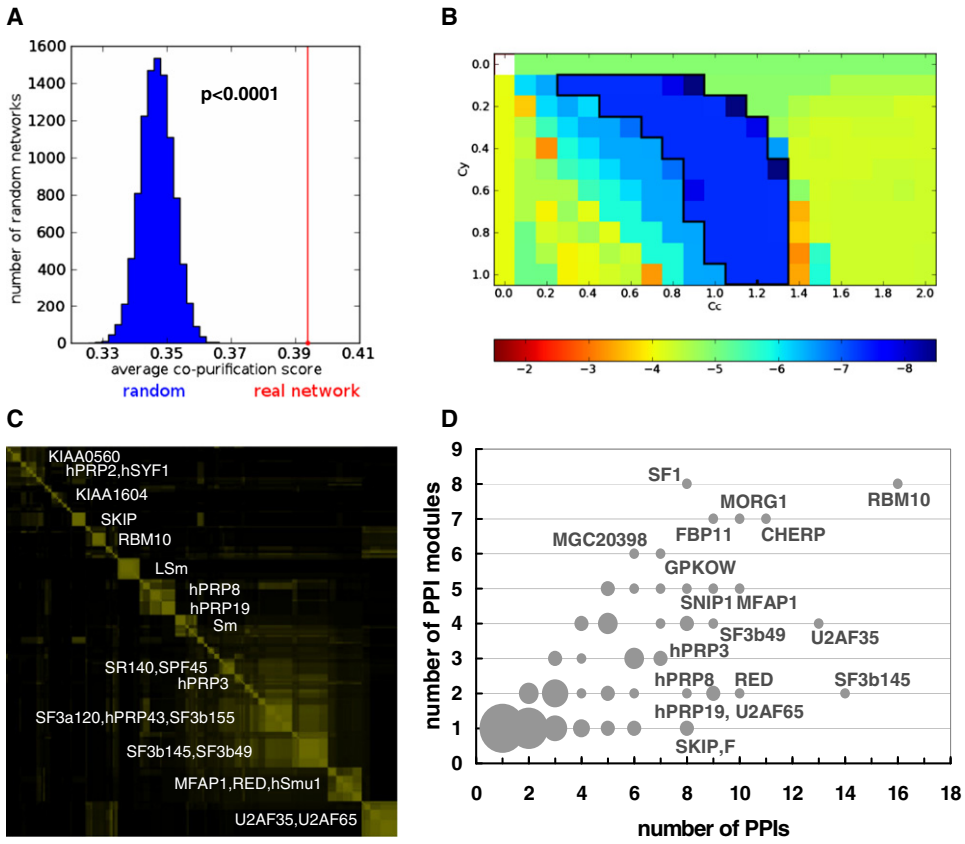

Figure 5. Cluster-Based Analysis of PPI Dynamics

(A) Comparison of the Y2H PPI data to copurification scores. The distribution of the average copurification scores of 10,000 randomly rewired networks is shown in comparison to the average of the real network (red line).

(B) Integration of Y2H and copurification data in a Markov clustering approach. The Y2H and copurification score factors (C_y and C_c, respectively) were varied in an extensive grid search to find the optimal combination of Y2H and copurification link weights for clustering. For every combination of C_y and C_c, we tested how well the obtained PPI modules represent the functional groups. The heat map shows the common logarithm of the mean enrichment P-value (hypergeometric test), with the most significant clustering results boxed.

(C) Interaction coclustering frequency matrix. The matrix represents all 231 core PPIs on x and y axis, with the color intensity indicating how often two interactions occurred together in PPI modules in the Markov clustering results with the best enrichment values. PPI modules with more than two PPIs (35) are on the diagonal. Proteins contributing the most PPIs to the modules are indicated (see Figure S3).

(D) Scatter plot showing the number of PPIs against the number of PPI modules a protein participates in for all spliceosomal core proteins. The size of each point indicates the number of proteins it represents. A high relative number of PPI modules suggests that the protein may have different interaction partners at distinct stages.

dynamics that are potentially relevant for spliceosome assembly and catalysis.

To analyze our PPI data in the context of the most biologically relevant interaction modules, we combined the direct PPI information from our Y2H analysis with the co-complex purification information. The copurification information strengthens direct PPIs between proteins that preferentially copurify and weakens PPIs between proteins that copurify rarely. It also assigns nonzero weights to many protein pairs that were not found to interact in the Y2H screen. In an extensive grid search, we assessed varying contributions of the copurification score and the Y2H PPI data. The grid search matrix shows a defined area of the most significant clustering results (Figure 5B, boxed) that contains PPI modules most closely reflecting the functional grouping of the spliceosomal core proteins. We summarized the results in an interaction coclustering frequency matrix, where 35 modules containing 2 to 21 PPIs are apparent (Figure 5C). These modules (Figure S3) likely represent proteins interacting concurrently at a particular stage during splicing.

This clustering approach provided clues to PPI dynamics during spliceosome assembly/function. First, a set of proteins is contained in relatively many modules. For example, proteins like GPKOW, SNIP, MFAP1, SF3b49, U2AF35, hPRP3, or hPRP8 participate in two or more modules (Figure 5D). In agreement with the spliceosome's highly dynamic protein composition, such proteins are candidates for recruiting different partners during the splicing cycle or are potential sites for major rearrangements (Figure 5D). Second, PPI modules with overlapping protein compositions were clearly separated from one another or showed mutually exclusive connections. For

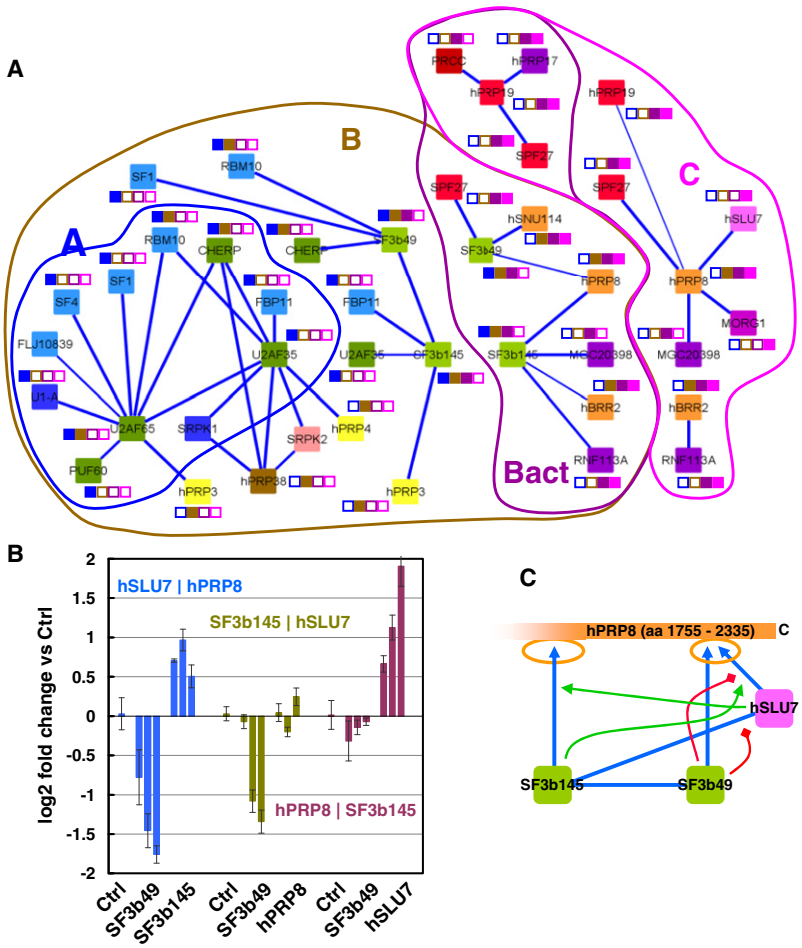

Figure 6. PPI Dynamics Involving SF3b Proteins and hPRP8

(A) Network representation of PPI dynamics involving SF3b-complex proteins and hPRP8. Selected PPIs from the (U2AF35 and U2AF65), the (SF3b145 and SF3b49), the hPRP19, and the hPRP8 modules are shown (c.f., Figure 5C). Please note that some proteins occur more than once in the network (SF3B49, SF3b145, hPRP8, etc.) as interactions were clustered and proteins contributed PPIs to different modules. Distinct PPI patterns for proteins are suggested for different stages (i.e., A, B, Bact, and C complexes) of the spliceosomal assembly cycle. The abundance of the proteins in the complexes as measured by (Agafovnov et al., 2011) is indicated through a box code next to the proteins. A filled colored box indicates high abundance, and an open box indicates low abundance or destabilization of the protein in the A (blue), B (brown), Bact (violet), and C (magenta) complexes, respectively.

(B) Competitive binding measured in a dose-dependent manner in co-IP assays. Increasing amounts of FLAG-tagged protein-coding plasmid DNAs were cotransfected with the protein A- and firefly-tagged interaction partners. Log_2-fold change of binding for the indicated protein pair in comparison to binding in the absence of a third protein (Ctrl) was calculated from relative luciferase intensities; error bars show the SD from triplicate transfections.

(C) The network schema summarizes the experiments indicating stimulation of binding by green arrows and binding competition by red diamond-headed lines.

example, we find a PPI module in which U2-related proteins, such as U2FAF35 and CHERP, are connected to A and U1 proteins (Figure 6A). They also interact with the U2 proteins SF3b145 and SF3b49. However, in a separate module these two SF3b proteins interact with the U5 proteins hPRP8, hBRR2, or hSNU114 (Figure 6A). These distinct PPI modules involving SF3b145 and SF3b49 may reflect rearrangements in their interaction partners during the transition from the A to B or from B to Bact complex. During these steps, SF3b interactions with U2-related proteins might be replaced by interactions with U5 proteins. Interestingly, the U5–SF3b-complex PPI module is also separated from a module containing hPRP8 interactions with hPRP19 complex, C complex, and second-step proteins, such as MORG1 and hSLU7. The latter suggest that PPIs involving hPRP8 are dynamic during the transition from the Bact to C complex (Figure 6A), with U5–U2 SF3b protein contacts replaced by second-step and C proteins.

Assaying PPI Dynamics in Competitive Coimmunoprecipitation Assays

Our clustering analyses suggest that hPRP8 changes interaction partners during the B to C complex transition. The hPRP8 core/MPN domain fragment (aa 1755–2335) contains the interaction site for SF3b145 and SF3b49, and also for hSLU7. To provide experimental evidence for the dynamic PPI rearrangements proposed here, we tested the binding of these three proteins to the hPRP8 fragment in a competition assay (Figure 6B). The binding of two proteins was measured using the luciferase-based co-IP assay in the presence of increasing amounts of a third cotransfected FLAG-tagged protein. The assay allowed us to determine both positive and negative effects of the third protein on the binding of the other two proteins in a dose-dependent manner. hSLU7 and SF3b145 stimulated each other's binding to hPRP8. Conversely, the hSLU7–hPRP8 interaction was inhibited by SF3b49 (Figure 6C). Interestingly, although SF3b145 interacts with hSLU7, SF3b49 competes for the hSLU7-SF3b145 interaction in a dose-dependent manner, suggesting that this PPI is weaker than SF3b145-SF3b49 binding. These experiments support the hypothesis that the hSLU7-hPRP8 interaction could replace the SF3b49-hPRP8 interaction during C complex formation.

We also observed that the DEAH-type RNA helicase proteins, hPRP2 and hPRP16, which are ATP-dependent rate-limiting first- and second-step proteins, respectively (Lardelli et al., 2010; Zhou and Reed, 1998), interact with GPKOW and form a PPI module (c.f., Figure 5C). In contrast, hPRP43 and hPRP22, which are closely related in terms of sequence and domain structure (Silverman et al., 2003), do not bind GPKOW. We tested hPRP2 and hPRP16 in competitive co-IP assays for their interaction with GPKOW and used the highly sequence-related hPRP43 as a specificity control (Figure 7A). Interestingly, hPRP16 strongly reduces hPRP2-GPKOW binding but cannot outcompete hPRP2 completely in these experiments. On the

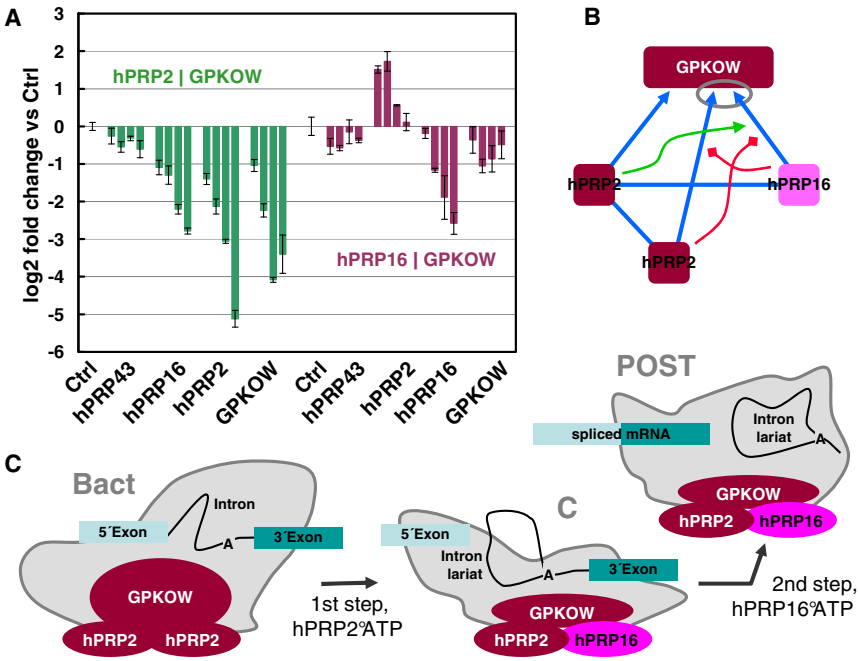

Figure 7. Ordered hPRP2 and hPRP16 Action

(A) Competition assays with hPRP2 and hPRP16 assaying GPKOW binding. Increasing amounts of FLAG-tagged protein-coding plasmid DNAs were cotransfected with the protein A- and firefly-tagged interaction partners. Log_2-fold change of binding for the indicated protein pair in comparison to binding in the absence of a third protein (Ctrl) was calculated from relative luciferase intensities; error bars show the SD from triplicate transfections. The sequence-related hPRP43 served as specificity control. The assay gave essentially identical results in the presence of 2mM ATP.

(B) Results from (A) are summarized in the network schema.

(C) Working model for ordered hPRP2 and hPRP16 action. During the first step of catalysis, which is driven by hPRP2 in an ATP-dependent manner, the spliceosome undergoes conformational rearrangements. The model proposes that hPRP2 acts at higher stoichiometry during this step. At least one copy of hPRP2 remains bound after the first step and stimulates hPRP16 binding to GPKOW. hPRP16 catalyzes the second step (exon joining) of splicing in an ATP-dependent manner. Here, hPRP16 action requires bound hPRP2 and works in an analogous fashion to hPRP2.

other hand, hPRP2 stimulates hPRP16 binding to GPKOW only when present in low amounts (Figure 7B). This suggests that hPRP16 may require bound hPRP2 for its interaction with GPKOW and that GPKOW serves as the recruitment site for both of these ATP-dependent helicases (Figure 7C and discussion).

DISCUSSION

Comprehensive PPI Wiring of the Human Spliceosome

To better understand the compositional and structural dynamics of the human spliceosome, we systematically analyzed PPIs between a comprehensive set of human spliceosomal proteins. Although the spliceosome is an RNP with large protein content, both in terms of protein number and mass, prior to this study there was very limited information about direct PPIs in the spliceosome. Thus, we performed an extensive Y2H matrix analysis involving 3–6 repeats of systematically screening all pairwise combinations of 237 spliceosomal core and noncore proteins for interaction (Figures 1 and 2). This approach resulted in a high-quality network of 632 interactions between 196 proteins. Among these, 390 PPIs involved noncore proteins and 242 PPIs were reported between spliceosomal core proteins. Benchmarking against re-evaluated literature-derived data demonstrated exceptionally high coverage of known interactions (Figure 3A). We recapitulated 41% of the known interactions between core spliceosomal proteins and at the same time expanded the spliceosomal PPI knowledge significantly. There is excellent agreement with the knowledge-based functional annotation of the proteins and the PPI data. Proteins belonging to the same operationally defined group interact preferentially (Figure 3B). In a standardized co-IP assay, the validation rate is high and essentially comparable to the validation rate of literature interactions (Venkatesan et al., 2009), providing additional support for the high quality of the data. Thus, this data set is a very reliable resource that will promote further investigation and analysis of the function of spliceosomal proteins. As with any screening approach that establishes a data-rich resource, individual PPI results will require additional validation via directed experiments that go beyond physical PPI testing by attempting to analyze the functional consequences of the interactions.

PPIs Potentially Involved in Tri-snRNP and Prp19 Complex Integration

Despite the fact that the tri-snRNP is protein-rich and PPIs were thought to play a key role in its recruitment and stable association with the spliceosomal B complex, little is known about this essential step. The U2-related protein SPF30 was previously shown to aid tri-snRNP association, apparently via its interaction with the U4/U6-PRP3 (Meister et al., 2001; Rappsilber et al., 2001), a PPI recapitulated in our study (Table S3). Furthermore, the tri-snRNP proteins hSAD1 and hSNU66 were also implicated in tri-snRNP addition (Makarova et al., 2001). We identify 5 PPIs involving hSNU66, including one with MFAP1, an abundant B-complex protein. Phosphorylation of three tri-snRNP proteins (hPrp28, hPRP6, and hPRP31) has also been linked to stable tri-snRNP integration in the B complex (Mathew et al., 2008; Schneider et al., 2010). Interestingly, we detected an interaction between hPRP6 and the B complex protein RED. RED interacts with the B complex proteins hSmu-1 and MFAP1, with the latter binding, in turn, to hPRP3 (Figure 4A). Thus, this group of

B complex proteins may be involved in tri-snRNP addition, and it is conceivable that phosphorylation of hPRP6 could potentially enhance this involvement. Our data further suggest that the identified PPIs between U2-SF3b proteins (which as major components are already present in the A complex) and the U5 proteins hPRP8, hBRR2, and hSNU114, likely also contribute to the recruitment of the tri-snRNP. SF3b proteins, such as SF3b145 and SF3b49, have been shown to contact the pre-mRNA several nucleotides upstream of the branchpoint (Gozani et al., 1996). In agreement with the found contacts, U5 proteins, such as hPRP8 and hBRR2, are also thought to be located at or near the spliceosome's catalytic core (Abelson, 2008).

PPIs, which are important for Prp19 complex recruitment and stable association after spliceosome activation, are poorly understood, but of high significance given the essential role that this complex plays in spliceosome activation. Our data suggest that the initial docking of the Prp19 complex during B complex formation may involve hPRP19 interactions with the A complex proteins RBM5 and RBM10 (Figure 4A) and potentially also U2 and U2-related proteins, as suggested by PPIs between AD002-SPF45 or PRL1-SF3b155. Interactions involving the PRP19-related proteins hSYF1 and SKIP, and RED and MFAP1, respectively, suggest that the latter B complex proteins may help recruit PRP19-related proteins. Additional interactions of hPRP19 and SPF27 with hPRP8 may also play an important role at this or later stages of splicing, whereas the hPRP19-hPRP17 interaction may be important for Prp19 complex stabilization during activation (Figure 4A).

PPIs Involving Noncore Spliceosomal Proteins

In addition to revealing multiple PPIs between spliceosomal core proteins, our interaction studies also shed light on a large number of previously unknown PPIs involving noncore spliceosomal proteins (Figure S4). These PPIs can provide initial indications about their potential function in splicing and how they connect with the spliceosome core components. For example, multiple PPIs involving noncore proteins found in low abundance in the C complex (Figure 1, C2) were detected between these proteins and core Bact and C complex proteins (Figure S4E), consistent with the idea that some C2 proteins associate with the spliceosome as preformed complexes. PPIs involving noncore splicing regulators (Figure 1, hnRNP, SR, MISC) can provide insight into their potential mechanism of action. For example, Fox-2 controls the alternative splicing of many exons in neurons, muscle, and other tissues by interacting with specific RNA sequences in the pre-mRNA (Zhang et al., 2008). Only a handful of proteins are known to interact with Fox-2, including hnRNPF (Mauger et al., 2008), an interaction recapitulated here. Our data reveal additional PPIs involving Fox-2, including those with hnRNPK and Sam68 (both known regulators of alternative splicing; (Chawla et al., 2009; Venables et al., 2008) and U1-C, that provide a basis for future studies aimed at unraveling its mechanism of action (Figures S4C and S4D).

Dynamic hPRP8 Interaction Partners during the Splicing Cycle

To better understand the interaction dynamics in the spliceosome, we employed an integrative clustering strategy combining our PPI data with a large spliceosomal-complex purification data set. The obtained PPI modules organize the core protein data into groups of interactions likely concurrent at distinct stages of splicing (Figure S3).

Our clustering analysis provided evidence that SF3b145, SF3b49, and hPRP8 may engage in different mutually exclusive PPIs during the transition from A/B to Bact and Bact to C complexes, respectively (Figure 6A). The interactions of SF3b145 with U2AF35 and of SF3b49 with CHERP are found in a module that is present in the A and, potentially, the B complex. U2-related proteins are released during the reorganization of the RNA and the PPI network from the B to the Bact complex (Bessonov et al., 2010). Therefore, these PPIs must be disrupted at some point during the transition from A to Bact, with the establishment of U2–U5 contacts potentially playing a major role in the new complex. Of course, we cannot rule out that some of these PPIs occur concomitantly because proteins will also bind simultaneously to multiple partners. Interactions between U5 proteins (hBRR2, hPrp8, and hSNU114) and SF3b subunits (SF3b145, SF3b49, and SF3b130) must be established in the B or Bact complex (i.e., prior to the first step of splicing). Approximately 30 proteins are recruited during the transition to the C complex (Bessonov et al., 2010), including second-step factors (like hSLU7) and C complex proteins, whereas SF3a/b proteins are at least partially destabilized or released (Bessonov et al., 2010). Our data indicate that the hPRP8 interactions with SF3b49 and SF3b145 may be replaced by PPIs with C and second-step proteins, such as MORG1 and hSLU7. Specifically, we propose that the hPRP8 interaction with SF3b49 is replaced by the hPRP8- hSLU7 interaction, a hypothesis supported by competition assays (Figure 6). Interestingly, hSLU7 interacts with the region of hPrp8 proposed to be localized at/near the spliceosome's active site (i.e., its RNase H-like domain [Pena et al., 2008; Ritchie et al., 2008; Yang et al., 2008]). Thus, the hSLU7-hPRP8 interaction described here would position hSLU7 near the catalytic core, potentially prior to its action during the second step of splicing. By binding close to the catalytic site, SLU7 might help to position the 3′ss for catalytic step II or stabilize the step II conformation of the spliceosome (Konarska and Query, 2005). Taken together, our results are consistent with the idea that dynamic PPIs involving a defined region of hPRP8 play an important role during spliceosome assembly/function.

Ordered hPRP2 and hPRP16 Action through GPKOW Binding

DEAH-box helicases play crucial roles in triggering rearrangements during the spliceosomal assembly cycle. The GPKOW ortholog, Spp2, is known to recruit PRP2 in yeast (Silverman et al., 2004) during the transition from Bact to B* complex. Both proteins are required for step I catalysis (Gencheva et al., 2010; Warkocki et al., 2009). PRP16, which follows PRP2 action, catalyzes the step II (Schwer and Guthrie, 1992; Zhou and Reed, 1998). While the requirement of GPKOW for PRP2 binding and step I catalysis is well documented, no analogous PPI partner for PRP16 has been suggested. We found in our analyses that hPRP16 also interacts with GPKOW and that hPRP2 and hPRP16 bind each other. Surprisingly, hPRP2 stimulated

hPRP16-GPKOW binding when coexpressed at low amounts, whereas hPRP16 competed with the hPRP2-GPKOW interaction but could not completely displace hPrp2 (Figure 7). The co-IP signal for hPRP2 binding to GPKOW was very high at a comparable expression level (Table S6). A simple model based on these findings (Figure 7C) suggests that GPKOW binds more than one copy of hPRP2 in the spliceosome during the first step. Greater than 1:1 hPRP2 / GPKOW stoichiometry would promote the rearrangements leading to step I. For step II, hPRP2 would be partially replaced by hPRP16, a rearrangement potentially facilitated by step I conformational changes. Importantly, however, at least one copy of hPRP2 would remain bound, which would promote hPRP16-binding to GPKOW at this stage. By remaining bound after step I, hPRP2 might ensure that hPRP16 acts in a consecutive manner and at a similar site, namely as a second-step ATP-dependent helicase after hPRP2 action. In strong support of this model, the abundance of hPRP2 decreases (close to 50%) during the Bact to C complex transition but a considerable fraction of hPRP2 remains bound (Agafonov et al., 2011). Two recent reports indicate a proofreading role for PRP16 in the first catalytic step of splicing in *S. cerevisiae* (Koodathingal et al., 2010; Tseng et al., 2011), suggesting a functional link between PRP2 and PRP16, at least in yeast. An alternative interpretation of the two studies (Horowitz, 2011) suggests that, for slowly splicing substrates, PRP16 may function as a step I expeditor by releasing proofreading proteins. These recent data are consistent with our hypothesis that hPRP2 and hPRP16 act consecutively at the same site, probably in an analogous fashion, whereby hPRP16 action would require hPRP2.

EXPERIMENTAL PROCEDURES

Clones

Open reading frames (ORFs) were either obtained in a Gateway Entry vector or amplified via PCR and transferred to an Entry vector (pDONR221) in a BP cloning reaction. The ORFs were shuttled to Gateway destination vectors (i.e., lexA- [bait], Gal4AD- [prey], protein A-, firefly-, FLAG- expression vectors) using standard procedures (Invitrogen).

Y2H Analysis

PPI screening was performed as described previously with minor modifications (Stelzl et al., 2005; Vinayagam et al., 2011). Nonautoactivating baits (L40ccU MATa yeast strains) were mated with prey strains at least three times using independently transformed bait and prey yeast colonies (384 array format). Interacting bait-prey pairs were identified by growth on selective agar plates (Leu-Trp-Ura-His) and/or lacZ reporter gene activation assays. Only bait-prey pairs that showed growth at least two times were considered for statistic evaluation. As multiple clones and configurations of the same protein pair were tested in several replicas, we combined all data to obtain a normalized result for each interacting pair (Y2H score) according to the formula:

$$\text{Y2H score} = 1 - \prod_{i=1}^{n}(1 - p_i)$$

n being the number of bait-prey pairs that represent a unique PPI on ENTREZ GeneID level; and p_i being the fraction of a bait-prey pair found over bait-prey pair tested.

The PPI data are reported in Table S3 and have been submitted to the IMEx consortium through MINT database (assigned identifier IM-16179). They will be available in a searchable format at http://cpdb.molgen.mpg.de/spliceosome.

Coimmunoprecipitation/Binding Competition Assays

For co-IP assay, $25*10^4$ HEK293 cells in a well of a 96-well plate were transiently transfected with 16–50 ng of firefly- and PA-plasmid DNA using Lipofectamine 2000 (Invitrogen). For competition assays, 5–100 ng of FLAG-plasmid DNA were cotransfected with a constant amount of Firefly- and PA-plasmid DNA, and unrelated DNA was added to a total of 150 ng/well. Cells were lysed in 100 μl HEPES-buffer [50 mM HEPES (pH 7.4), 150 mM NaCl, 1 mM EDTA, 10% glycerol, 1% Triton X-100, 50 μg/ml RNase A, Protease Inhibitor (Roche, 11051600)] 24–36 hr after transfection for 30 min at 4°C. Protein complexes were precipitated from 70 μl cleared-cell extract in IgG-coated microtiter plates for 1hr at 4°C and washed 3× with 100 μl ice-cold PBS. The binding of the firefly-V5-tagged fusion protein (co-IP) to the PA-tagged fusion protein (IP) was assessed by measuring the firefly luciferase activity in a luminescence plate reader (Beckmann DTX800, Bright-Glo Luciferase Assay [Promega]). Assays were performed with triplicate transfections. Relative expression levels of the FLAG-tagged proteins (competition) and PA/fire-tagged proteins were monitored by western blotting. Log_2-fold change binding for the protein pair was calculated from relative luciferase intensities in comparison to background binding measured in parallel with the firefly-tagged and a nonrelated protein-A fusion protein. Ratios larger than two and a z-score larger than two were considered positive (Table S6).

Copurification Score

Spliceosomal complex purifications were summarized in a binary matrix K with columns corresponding to the purifications and rows corresponding to different proteins that were identified by MS at least once with at least one peptide. If a protein p was detected in a purification i, then $K_{ip} = 1$; otherwise $K_{ip} = 0$. Based on this matrix, a copurification score $C(p,q)$ was calculated for all pairs of proteins p and q using the formula:

$$C(p,q) = \frac{\sum_i \frac{K_{ip}K_{iq}}{\sum_j K_{ij} - 1}}{\sqrt{\sum_i K_{ip} \sum_i K_{iq}}}$$

Nonzero scores of spliceosomal protein pairs were rescaled to (0.0,1.0] through division by the maximum score. The scores show a broad distribution with an average of 0.36 (for details, see Figure S2).

PPI Clustering

Copurification scores were integrated with Y2H PPI information using the formula:

$$s(p,q) = 1 - \left(1 - C_y * Y[p,q]\right) * \left(1 - C_c * C[p,q]\right)$$

For each protein pair (p,q), the interaction weight $Y(p,q)$ was set to 1 if there was a direct PPI between p and q, and to 0 for noninteracting pairs. $C(p,q)$ is the copurification score for the protein pair. C_y and C_c are coefficients weighting the two lines of interaction evidence. Each combination of C_y and C_c yields a distinct set of protein-protein interaction weights $S(i,j)$, which is represented as a matrix S. A grid search for the coefficients C_y and C_c was performed in the intervals C_y (in) [0.0:1.0] and C_c (in) [0.0:2.0].

For each matrix S, we applied the original implementation (version 10-201) of the Markov clustering algorithm (Van Dongen, 2000) on the line graph of the interaction network given by S. The line graph of an interaction network represents nodes as interactions and edges as shared proteins. Edge weights in the line graph were defined as the mean score $S(i,j)$ of the incident interaction nodes. The inflation parameter of the Markov clustering, which essentially controls the number and size of the clusters, was chosen for each C_y / C_c combination to give rise to 20 clusters. The resulting clusters comprise direct PPIs, as well as many copurification relationships without direct interaction evidence.

Each cluster was translated to a nonweighted set of proteins that participate in at least one direct interaction and the overlap with each functional group of spliceosomal proteins was assessed using the hypergeometric test. The minimum p value per functional group points to a cluster that best resembles that group. The harmonic mean of the minimum p values for all functional

groups reflects the overall concordance of a clustering result with the known functional classes of spliceosomal proteins.

To identify PPI modules, we focused on the 51 clustering results with the lowest hypergeometric p values (boxed in Figure 5B). We additionally clustered the corresponding matrices S from these C_y / C_c combinations with a different inflation parameter to obtain 40 clusters. This reveals a more detailed organization of the PPI modules. All clustering results, with 20 and 40 clusters, from the 51 C_y / C_c combinations were used to derive an PPI co-clustering matrix, which contains the frequencies at which pairs of interactions were clustered together (Figure 5C).

SUPPLEMENTAL INFORMATION

Supplemental Information includes four figures and six tables and can be found with this article online at doi:10.1016/j.molcel.2011.12.034.

ACKNOWLEDGMENTS

We thank Sergey Bessonov for critical discussions and very helpful comments. The work was funded by the Max-Planck Society and the IMPRS-CBSC (A.K.).

Received: August 19, 2011
Revised: November 1, 2011
Accepted: December 12, 2011
Published: February 23, 2012

REFERENCES

Abelson, J. (2008). Is the spliceosome a ribonucleoprotein enzyme? Nat. Struct. Mol. Biol. *15*, 1235–1237.

Agafonov, D.E., Deckert, J., Wolf, E., Odenwälder, P., Bessonov, S., Will, C., Urlaub, H., and Luhrmann, R. (2011). Semi-quantitative proteomic analysis of the human spliceosome via a 1 novel two-dimensional 2 gel electrophoresis method. in press.

Bessonov, S., Anokhina, M., Will, C.L., Urlaub, H., and Lührmann, R. (2008). Isolation of an active step I spliceosome and composition of its RNP core. Nature *452*, 846–850.

Bessonov, S., Anokhina, M., Krasauskas, A., Golas, M.M., Sander, B., Will, C.L., Urlaub, H., Stark, H., and Lührmann, R. (2010). Characterization of purified human Bact spliceosomal complexes reveals compositional and morphological changes during spliceosome activation and first step catalysis. RNA *16*, 2384–2403.

Chawla, G., Lin, C.H., Han, A., Shiue, L., Ares, M., Jr., and Black, D.L. (2009). Sam68 regulates a set of alternatively spliced exons during neurogenesis. Mol. Cell. Biol. *29*, 201–213.

Chua, K., and Reed, R. (1999). Human step II splicing factor hSlu7 functions in restructuring the spliceosome between the catalytic steps of splicing. Genes Dev. *13*, 841–850.

Corsini, L., Bonnal, S., Basquin, J., Hothorn, M., Scheffzek, K., Valcárcel, J., and Sattler, M. (2007). U2AF-homology motif interactions are required for alternative splicing regulation by SPF45. Nat. Struct. Mol. Biol. *14*, 620–629.

Fromont-Racine, M., Rain, J.C., and Legrain, P. (1997). Toward a functional analysis of the yeast genome through exhaustive two-hybrid screens. Nat. Genet. *16*, 277–282.

Gabellini, D., D'Antona, G., Moggio, M., Prelle, A., Zecca, C., Adami, R., Angeletti, B., Ciscato, P., Pellegrino, M.A., Bottinelli, R., et al. (2006). Facioscapulohumeral muscular dystrophy in mice overexpressing FRG1. Nature *439*, 973–977.

Gehring, N.H., Lamprinaki, S., Kulozik, A.E., and Hentze, M.W. (2009). Disassembly of exon junction complexes by PYM. Cell *137*, 536–548.

Gencheva, M., Kato, M., Newo, A.N., and Lin, R.J. (2010). Contribution of DEAH-box protein DHX16 in human pre-mRNA splicing. Biochem. J. *429*, 25–32.

Gozani, O., Feld, R., and Reed, R. (1996). Evidence that sequence-independent binding of highly conserved U2 snRNP proteins upstream of the branch site is required for assembly of spliceosomal complex A. Genes Dev. *10*, 233–243.

Grote, M., Wolf, E., Will, C.L., Lemm, I., Agafonov, D.E., Schomburg, A., Fischle, W., Urlaub, H., and Lührmann, R. (2010). Molecular architecture of the human Prp19/CDC5L complex. Mol. Cell. Biol. *30*, 2105–2119.

Horowitz, D.S. (2011). The splice is right: guarantors of fidelity in pre-mRNA splicing. RNA *17*, 551–554.

Jurica, M.S., and Moore, M.J. (2003). Pre-mRNA splicing: awash in a sea of proteins. Mol. Cell *12*, 5–14.

Kamburov, A., Pentchev, K., Galicka, H., Wierling, C., Lehrach, H., and Herwig, R. (2011). ConsensusPathDB: toward a more complete picture of cell biology. Nucleic Acids Res. *39* (Database issue), D712–D717.

Konarska, M.M., and Query, C.C. (2005). Insights into the mechanisms of splicing: more lessons from the ribosome. Genes Dev. *19*, 2255–2260.

Koodathingal, P., Novak, T., Piccirilli, J.A., and Staley, J.P. (2010). The DEAH box ATPases Prp16 and Prp43 cooperate to proofread 5′ splice site cleavage during pre-mRNA splicing. Mol. Cell *39*, 385–395.

Lardelli, R.M., Thompson, J.X., Yates, J.R., III, and Stevens, S.W. (2010). Release of SF3 from the intron branchpoint activates the first step of pre-mRNA splicing. RNA *16*, 516–528.

Lehner, B., and Sanderson, C.M. (2004). A protein interaction framework for human mRNA degradation. Genome Res. *14*, 1315–1323.

Liu, S., Rauhut, R., Vornlocher, H.P., and Lührmann, R. (2006). The network of protein-protein interactions within the human U4/U6.U5 tri-snRNP. RNA *12*, 1418–1430.

Makarova, O.V., Makarov, E.M., and Lührmann, R. (2001). The 65 and 110 kDa SR-related proteins of the U4/U6.U5 tri-snRNP are essential for the assembly of mature spliceosomes. EMBO J. *20*, 2553–2563.

Mathew, R., Hartmuth, K., Möhlmann, S., Urlaub, H., Ficner, R., and Lührmann, R. (2008). Phosphorylation of human PRP28 by SRPK2 is required for integration of the U4/U6-U5 tri-snRNP into the spliceosome. Nat. Struct. Mol. Biol. *15*, 435–443.

Mauger, D.M., Lin, C., and Garcia-Blanco, M.A. (2008). hnRNP H and hnRNP F complex with Fox2 to silence fibroblast growth factor receptor 2 exon IIIc. Mol. Cell. Biol. *28*, 5403–5419.

Meister, G., Hannus, S., Plöttner, O., Baars, T., Hartmann, E., Fakan, S., Laggerbauer, B., and Fischer, U. (2001). SMNrp is an essential pre-mRNA splicing factor required for the formation of the mature spliceosome. EMBO J. *20*, 2304–2314.

Nesic, D., and Krämer, A. (2001). Domains in human splicing factors SF3a60 and SF3a66 required for binding to SF3a120, assembly of the 17S U2 snRNP, and prespliceosome formation. Mol. Cell. Biol. *21*, 6406–6417.

Pena, V., Liu, S., Bujnicki, J.M., Lührmann, R., and Wahl, M.C. (2007). Structure of a multipartite protein-protein interaction domain in splicing factor prp8 and its link to retinitis pigmentosa. Mol. Cell *25*, 615–624.

Pena, V., Rozov, A., Fabrizio, P., Lührmann, R., and Wahl, M.C. (2008). Structure and function of an RNase H domain at the heart of the spliceosome. EMBO J. *27*, 2929–2940.

Pereira-Leal, J.B., Enright, A.J., and Ouzounis, C.A. (2004). Detection of functional modules from protein interaction networks. Proteins *54*, 49–57.

Rappsilber, J., Ajuh, P., Lamond, A.I., and Mann, M. (2001). SPF30 is an essential human splicing factor required for assembly of the U4/U5/U6 tri-small nuclear ribonucleoprotein into the spliceosome. J. Biol. Chem. *276*, 31142–31150.

Ren, L., McLean, J.R., Hazbun, T.R., Fields, S., Vander Kooi, C., Ohi, M.D., and Gould, K.L. (2011). Systematic two-hybrid and comparative proteomic analyses reveal novel yeast pre-mRNA splicing factors connected to Prp19. PLoS ONE *6*, e16719.

Ritchie, D.B., Schellenberg, M.J., Gesner, E.M., Raithatha, S.A., Stuart, D.T., and Macmillan, A.M. (2008). Structural elucidation of a PRP8 core domain from the heart of the spliceosome. Nat. Struct. Mol. Biol. *15*, 1199–1205.

Sanderson, C.M. (2009). The Cartographers toolbox: building bigger and better human protein interaction networks. Brief. Funct. Genomics Proteomics *8*, 1–11.

Sapra, A.K., Khandelia, P., and Vijayraghavan, U. (2008). The splicing factor Prp17 interacts with the U2, U5 and U6 snRNPs and associates with the spliceosome pre- and post-catalysis. Biochem. J. *416*, 365–374.

Schneider, M., Hsiao, H.H., Will, C.L., Giet, R., Urlaub, H., and Lührmann, R. (2010). Human PRP4 kinase is required for stable tri-snRNP association during spliceosomal B complex formation. Nat. Struct. Mol. Biol. *17*, 216–221.

Schwartz, A.S., Yu, J., Gardenour, K.R., Finley, R.L., Jr., and Ideker, T. (2009). Cost-effective strategies for completing the interactome. Nat. Methods *6*, 55–61.

Schwer, B., and Guthrie, C. (1991). PRP16 is an RNA-dependent ATPase that interacts transiently with the spliceosome. Nature *349*, 494–499.

Schwer, B., and Guthrie, C. (1992). A conformational rearrangement in the spliceosome is dependent on PRP16 and ATP hydrolysis. EMBO J. *11*, 5033–5039.

Silverman, E., Edwalds-Gilbert, G., and Lin, R.J. (2003). DExD/H-box proteins and their partners: helping RNA helicases unwind. Gene *312*, 1–16.

Silverman, E.J., Maeda, A., Wei, J., Smith, P., Beggs, J.D., and Lin, R.J. (2004). Interaction between a G-patch protein and a spliceosomal DEXD/H-box ATPase that is critical for splicing. Mol. Cell. Biol. *24*, 10101–10110.

Smith, D.J., Query, C.C., and Konarska, M.M. (2008). "Nought may endure but mutability": spliceosome dynamics and the regulation of splicing. Mol. Cell *30*, 657–666.

Staley, J.P., and Guthrie, C. (1998). Mechanical devices of the spliceosome: motors, clocks, springs, and things. Cell *92*, 315–326.

Stelzl, U., and Wanker, E.E. (2006). The value of high quality protein-protein interaction networks for systems biology. Curr. Opin. Chem. Biol. *10*, 551–558.

Stelzl, U., Worm, U., Lalowski, M., Haenig, C., Brembeck, F.H., Goehler, H., Stroedicke, M., Zenkner, M., Schoenherr, A., Koeppen, S., et al. (2005). A human protein-protein interaction network: a resource for annotating the proteome. Cell *122*, 957–968.

Tseng, C.K., Liu, H.L., and Cheng, S.C. (2011). DEAH-box ATPase Prp16 has dual roles in remodeling of the spliceosome in catalytic steps. RNA *17*, 145–154.

Van Dongen, S. (2000). A cluster algorithm for graphs. In Report Information Systems. (Centrum voor Wiskunde en Informatica), http://cat.inist.fr/?aModele=afficheN&cpsidt=1409637.

Venables, J.P., Koh, C.S., Froehlich, U., Lapointe, E., Couture, S., Inkel, L., Bramard, A., Paquet, E.R., Watier, V., Durand, M., et al. (2008). Multiple and specific mRNA processing targets for the major human hnRNP proteins. Mol. Cell. Biol. *28*, 6033–6043.

Venkatesan, K., Rual, J.F., Vazquez, A., Stelzl, U., Lemmens, I., Hirozane-Kishikawa, T., Hao, T., Zenkner, M., Xin, X., Goh, K.I., et al. (2009). An empirical framework for binary interactome mapping. Nat. Methods *6*, 83–90.

Vinayagam, A., Stelzl, U., Foulle, R., Plassmann, S., Zenkner, M., Timm, J., Assmus, H.E., Andrade-Navarro, M.A., and Wanker, E.E. (2011). A directed protein interaction network for investigating intracellular signal transduction. Sci. Signal. *4*, rs8.

Vlasblom, J., and Wodak, S.J. (2009). Markov clustering versus affinity propagation for the partitioning of protein interaction graphs. BMC Bioinformatics *10*, 99.

Wahl, M.C., Will, C.L., and Lührmann, R. (2009). The spliceosome: design principles of a dynamic RNP machine. Cell *136*, 701–718.

Warkocki, Z., Odenwälder, P., Schmitzová, J., Platzmann, F., Stark, H., Urlaub, H., Ficner, R., Fabrizio, P., and Lührmann, R. (2009). Reconstitution of both steps of Saccharomyces cerevisiae splicing with purified spliceosomal components. Nat. Struct. Mol. Biol. *16*, 1237–1243.

Yang, K., Zhang, L., Xu, T., Heroux, A., and Zhao, R. (2008). Crystal structure of the beta-finger domain of Prp8 reveals analogy to ribosomal proteins. Proc. Natl. Acad. Sci. USA *105*, 13817–13822.

Zhang, C., Zhang, Z., Castle, J., Sun, S., Johnson, J., Krainer, A.R., and Zhang, M.Q. (2008). Defining the regulatory network of the tissue-specific splicing factors Fox-1 and Fox-2. Genes Dev. *22*, 2550–2563.

Zhou, Z., and Reed, R. (1998). Human homologs of yeast prp16 and prp17 reveal conservation of the mechanism for catalytic step II of pre-mRNA splicing. EMBO J. *17*, 2095–2106.